CCC 2008 - Challenges for Civil Construction
Torres Marques et al. (Eds)


# ANALYTICAL MODEL FOR BOND-SLIP OF HOOKED-END STEEL FIBRES

**Vítor M.C.F. Cunha*[1], Joaquim A.O. Barros*[2] and José Sena-Cruz*[3]**

* DEC, ISISE, School of Engineering, University of Minho
Campus de Azurem, 4800-058 Guimarães, Portugal
e-mail: [1]vcunha@civil.uminho.pt, [2]barros@civil.uminho.pt, [3]jsena@civil.uminho.pt,
web page: http://www.civil.uminho.pt/composites

**Keywords:** pullout, analytical model, hooked-end fibres, numerical simulation

**Summary:** *In this work an analytical model for obtaining the local bond stress-slip relationship of hooked-end steel fibres is presented. The mathematical representation of the pullout problem is described and the numerical algorithm of the model is detailed. Furthermore, the performance of the developed model is assessed using results obtained in fibre pullout experimental tests.*

## 1 INTRODUCTION

In fibre reinforced cement composite (FRC), the interface between fibre and cement paste is the weak link of its micro-structure. Therefore, understanding how this interface behaves is mandatory to predict the macro-mechanical properties of FRC. Moreover, with the outcome of rather innovative matrices, such as, fibre reinforced self-compacting concrete, the study of the fibre/matrix interfacial behaviour assumes a new interest. However, even in the research of modern materials there is not a straightforward experimental method to assess the bond-slip relationship of a fibre/matrix system. This "direct" method would require the evaluation of the interfacial crack initiation and, moreover, the continuous monitoring of the crack growth. For this kind of experimental monitoring it would be necessary the use, in simultaneous, of several equipment, such as, microscope, video camera recorder, during the loading process of the fibre pullout test.

Hence, the effectiveness of a given fibre as a medium of stress transfer is often assessed using a single fibre pullout test, where fibre slip is monitored as a function of the applied load on the fibre [1,2]. Moreover, the results of the pullout tests are used in the development of analytical and numerical models to assess the bond-slip relationship and the bond stress distribution along the fibre. Several authors have developed models for straight smooth fibres based on force equilibrium considerations and assuming the fibre pullout test as an axisymmetric stress and strain problem [3,4].
Nevertheless, the models for straight smooth fibres are of questionable application for hooked-end fibres, since the behaviour of hooked-end fibres is dominated by the mechanical anchorage. In hooked-end fibres the bond strength may be small when compared to the parcel provided by the mechanical anchorage. More recently, analytical models have been developed to predict the mechanical contribution of anchorage resistance assured by the hooked extremities of steel fibres [5,6].

The abovementioned analytical models are only capable to determine a load-slip relationship $N(s)$ of a pullout test adopting a bond law, $\tau(s)$, i.e. the direct problem, where with $\tau(s)$ the $N(s)$ is obtained. The straightforward analytical determination of the bond stress versus slip relationship for a given pullout curve, i.e. the inverse problem where with $N(s)$ is obtained $\tau(s)$, is extremely difficult due to considerable complexities from mathematical point-of-view [7]. Actually, to overcome this concern, the inverse problem was approached as a direct problem with an integrated numerical fitting tool.

In the present work an analytical cohesive interface model is developed to obtain the bond stress-

slip relationship for hooked ends steel fibres. To account for the interfacial bond, a non-linear bond stress-slip law was used. On the other hand, the reinforcement mechanism provided by the fibre mechanical anchorage was accounted by a nonlinear spring component. The mathematical representation of the pullout problem was based on a stress criterion supported on both the problem boundary conditions and a second order differential equation that governs the slip evolution of steel fibres. To solve this differential equation an iterative method (Newton-Raphson) and a numerical integration procedure (Runge-Kutta-Nyström) were used. In the present work the numerical method and the mathematical tools are detailed and its performance is assessed. Hence, the parameters that define the local bond stress-slip relationship are obtained by a fitting procedure between the simulated pullout curve and the experimental one.

## 2 OVERVIEW OF EXISTING FIBRE PULLOUT MODELS

One of the first pullout models was proposed by [8], which relates the shear stress distribution along the fibre to the elastic properties of the matrix and fibre. Based on the latter, several other models were developed for the fibre pullout problem [3,4,9,10]. These models are one-dimensional, with many common features. They include a shear-lag model for the fibre embedded length in full bond conditions, gradual debonding, and frictional sliding for the fibre embedded length where debonding is occurring. In [10] only frictional bond was considered. The force distribution in the fibre and matrix was deduced in [4]. A two-way debonding theory was developed in [11], in which the debonding can progress from both fibre ends. In other models, at a first stage, when fibre is fully bonded to the matrix, it is assumed that the interfacial shear bond stresses are elastic. After debonding takes place, two interfacial zones will arise, a bonding and debonding zone, in the latter the stress transfer will be governed by frictional shear bond [9]. To describe the debonding criterion, basically two different approaches have been used: a strength-based criterion (or stress-based) and a fracture-based criterion. In the strength based models, it is assumed that debonding initiates when the interfacial shear stress exceeds the shear strength. For the fracture-based models, the debonding zone is treated as an interfacial crack. To drive the debonded zone forward, i.e. interfacial crack propagation, the energy release rate for propagation of a unit length interfacial crack must be equal to the fracture energy resistance of the material, see [3,12]. Nevertheless, the models for straight fibres are of questionable use for hooked-end fibres, since the behaviour of hooked-end fibres is dominated by the mechanical anchorage. In hooked-end fibres the bond strength may be small when compared to the parcel provided by the mechanical bond [1,13]. An analytical model to predict the mechanical contribution of anchorage resistance assured by the hooked extremities of steel fibres was developed in [14]. The mechanical bond provided by the hook is considered as a function of the work needed to straighten the fibres during pullout. To predict the full pullout response a two-step process is needed, corresponding to the contribution of the frictional and mechanical components. To overcome this two-step process, an analytical model was developed in [15], where both the frictional bond and mechanical anchorage components are combined in the solution. This model is an extension of the smooth fibre pullout model, previously developed by [4], where the adoption of a nonlinear spring component intends to simulate the mechanical anchorage reinforcement mechanism.

## 3 THEORETICAL RELATIONSHIPS

The pullout problem is often represented by a second order differential equation, established in terms of forces [4,7,15]. Nevertheless, since in the model developed within the ambit of the present work the displacements of the concrete points at the interface between concrete and fibre were neglected, the differential equation was derived in terms of slip, after [16-18]. For hooked-end steel fibres aligned with the pullout force, the three bond mechanisms that during the pullout contribute to the ductility of the composite material are: adhesion, friction, mechanical bond. The first two components can be simulated by a local bond-slip relationship, whereas the mechanical bond due to the anchorage resistance at the fibre embedded end, can be simulated by an additional spring

component, Fig. 1. The pullout problem of hooked fibres is markedly a three dimensional problem. Even so, it was approached as a two dimensional problem, since otherwise it would be extremely difficult to plant an analytical model. Moreover, it seemed feasible to model the interfacial bond of the hooked fibre as a two dimensional axisymmetric problem, since the hook length is relatively smaller than the fibre length, and then introduce the anchorage component by a spring.

### 3.1 Local bond-slip

The equilibrium of the free body with an infinitesimal length *dx* of a fibre bonded to a concrete matrix can be given by (see Fig. 1(c)):

$$\sigma_f \cdot A_f + \tau \cdot P_f \cdot dx = \left(\sigma_f + d\sigma_f\right) \cdot A_f \tag{1}$$

where $\tau = \tau(s(x))$ is the local bond shear stress acting on the contact surface between fibre and concrete, and *s* is the slip, i.e. the relative displacement between the fibre and the concrete. Finally, $\sigma_f$, $A_f$ and $P_f$ are the normal stress, cross section area and perimeter of the fibre, respectively.

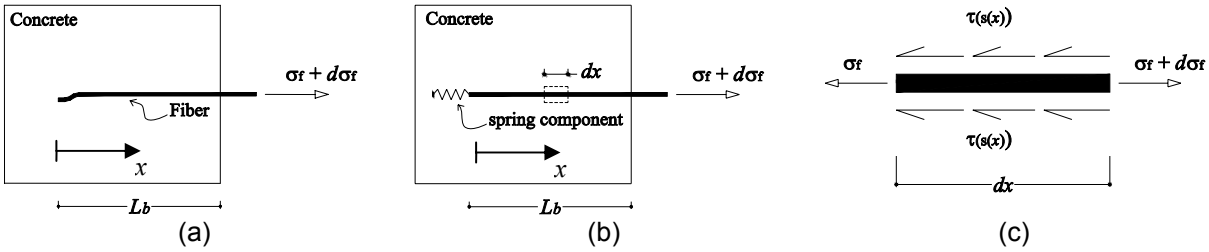


Figure 1: Axisymetric pullout model: (a) general problem, (b) simplified model (c) equilibrium of an infinitesimal fibre free-body.

Assuming that the fibre has a linear elastic constitutive law in the longitudinal direction ($d\sigma_f = E_f \cdot d\varepsilon_f$), Eq. 1 can be rewritten into:

$$\tau = \frac{E_f A_f}{P_f} \cdot \frac{d\varepsilon_f}{dx} \tag{2}$$

where $E_f$ and $d\varepsilon_f$ are, respectively, the Young modulus and the strain of the fibre. The strain components in a representative bulk of the fibre-concrete interface are indicated in Fig. 2. The slip variation over an infinitesimal length, *ds*/*dx*, is given by:

$$\frac{ds}{dx} = \varepsilon_f - \varepsilon_c \tag{3}$$

where $\varepsilon_c$ is the concrete strain. However, the contribution of the concrete deformability in the slip assessment may be neglected, since the fibre is subjected to large inelastic deformations. Several authors have neglected this component, on the evaluation of the bond-slip relationship of reinforcing bars [16] and FRP reinforcement [17,18]. To validate this assumption for small fibres, an analytical model was used, which takes into account the deformation of the matrix surrounding the fibre [15], in the assessment of the pullout force-slip relationship. A sensitivity analysis was carried out using the latter model to evaluate the influence of the matrix deformation on the pullout response. For the current fibres lengths and matrix stiffness, the $\varepsilon_c$ did not influence the slip value determination, since $\varepsilon_c << \varepsilon_f$.

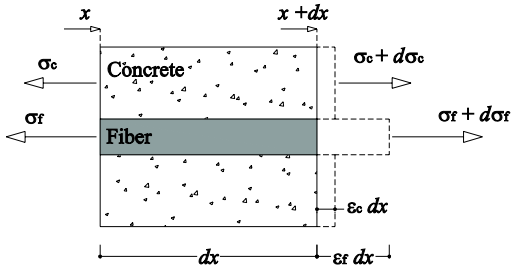


Figure 2: Stresses and strains on the fibre bond region.

Considering the abovementioned assumptions, neglecting the concrete deformability in the slip determination ( $\varepsilon_c = 0$ ), and incorporating Eq. 3 into Eq. 2, the second order differential equation that governs the local bond phenomena of the fibre-matrix interface is given by:

$$\frac{d^2 s}{dx^2} = \frac{P_f}{E_f A_f} \cdot \tau(x) \tag{4}$$

### 3.2 Pullout force-slip relationship

The pullout force-slip relationship can be determined using either an energy approach [17] or an equilibrium approach [4,16]. In the present work the energy approach is adopted.

Consider a steel fibre embedded on a concrete matrix over a bond length $\tilde{L}_b = L_b$, where *N* is the generic applied pullout force, and $s_f$ and $s_l$ are, respectively, the free and loaded end slips starting at the free end of the fibre (see Fig. 3). When the fibre is slipping due to an applied pullout force, *N*, the following functions can be evaluated along the fibre bond length: slip along the fibre, *s(x)*; bond shear stress along the embedded length, $\tau(x)$; fibre strain, $\varepsilon_f$; and the axial force, *N(x)*.

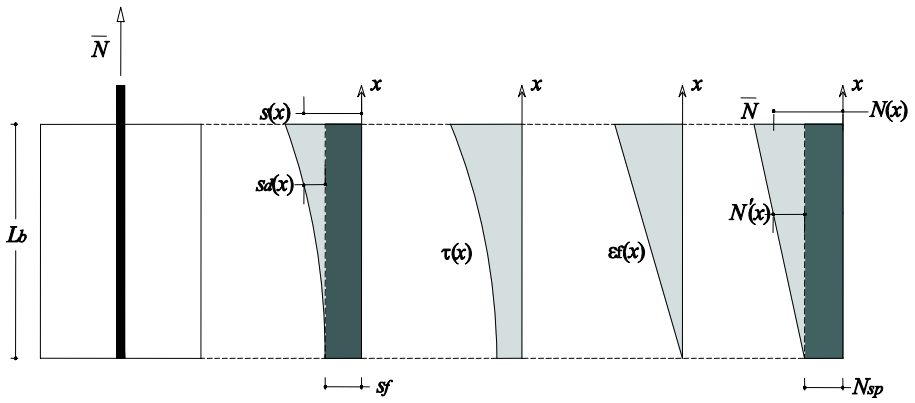


Figure 3: Entities evolved in the developed method.

In Fig. 3 the slip diagram along the fibre, *s(x)*, can be regarded as the sum of two components. A constant component, $s_f$, which produces a rigid body displacement of the fibre, whereas the $s_d(x)$ component results from the deformation of the fibre. Moreover, for any point *x* of the fibre embedded length, just the $s_d(x)$ component will result in a fibre length change, and, therefore, contributing to the fibre deformation energy. Likewise, the axial force along the fibre *N(x)* can be decomposed into two

components: a constant component, $N_{sp}$, due to the spring load (only in the case of hooked fibres) and the *N'(x)* component. Only the latter will contribute to the fibre deformation energy, since in the adopted model it was assumed that $N_{sp}$ does not produce a fibre length change. Therefore, the fibre deformation at a point *x* is obtained from $\varepsilon_f(x) = N'(x)/(E_f A_f)$. Considering a generic fibre cross section at the interval $0 \le x \le \tilde{L}_b$, and that the fibre lateral surface over embedded length $\overline{x}$ is $\Omega = P_f \cdot \overline{x}$, the work performed by external forces acting on the range $0 \le x \le \tilde{L}_b$ is:

$$w_{ext} = \int_{\Omega} \left( \int_{s_f}^{s(x)} \tau(s) \cdot ds \right) d\Omega = P_f \int_0^{\overline{x}} \left( \int_{s_f}^{s(x)} \tau(s) \cdot ds \right) dx \tag{5}$$

On the other hand, remarking $V_f = A_f \cdot \overline{x}$ as the fibre volume over the embedded length, the elastic energy of the fibre is:

$$\begin{aligned} w_{\text{int}} &= \int_{V_f} \left( \int_0^{\varepsilon(x)} \sigma_f(\varepsilon_f) \cdot ds \right) dV_f = A_f \int_0^{\overline{x}} \left( \int_0^{\varepsilon(x)} E_f \varepsilon_f \cdot d\varepsilon \right) dx \\ &= \frac{A_f}{2E_f} \int_0^{\overline{x}} \sigma_f^2(x) \cdot dx \end{aligned} \tag{6}$$

From Eq. 5 and 6 is obtained:

$$\int_0^{\overline{x}} \left( P_f \int_{s_f}^{s(x)} \tau(s) \cdot ds - \frac{A_f}{2E_f} \sigma_f^2(x) \right) dx = 0 \tag{7}$$

Since Eq. 7 must be satisfied for each value of $0 \le x \le \tilde{L}_b$, this equation may be rewritten as:

$$P_f \int_{s_f}^{s(x)} \tau(s) \cdot ds - \frac{A_f}{2E_f} \sigma_f^2(x) = 0 \tag{8}$$

At $x = \tilde{L}_b$ Eq. 8 becomes:

$$P_f \int_{s_f}^{s(x=\tilde{L}_b)} \tau(s) \cdot ds - \frac{N'^2}{2E_f A_f} = 0 \tag{9}$$

$$N' = \sqrt{2E_f \cdot A_f \cdot P_f \cdot \int_{s_f}^{s(x=\tilde{L}_b)} \tau(s) \cdot ds} \tag{10}$$

Eq. 10 allows determining the generic applied pullout force for a smooth fibre or, in the case of a hooked fibre, the pullout force component at the fibre free end due to the interfacial bond of the fibre. Regarding that in the case of hooked fibres, the generic applied load is $N = N' + N_{sp}$ (see Fig. 3), for these fibres the generic applied load is given by:

$$N' = \sqrt{2E_f \cdot A_f \cdot P_f \cdot \int_{s_f}^{s(x=\tilde{L}_b)} \tau(s) \cdot ds} + N_{sp} \tag{11}$$

## 4 DESCRIPTION OF THE ANALYTICAL MODEL

The adopted method is supported on the work developed by [17,18]. In order to improve the performance of the method and to adapt it to the specificities of the present study, some modifications were performed. In this section, it is described in detail the implemented algorithm.

Considering the entities described in Fig. 3, the boundary conditions at the free and loaded ends indicated in Eq. 12 can be stated for smooth fibres, whereas the boundary conditions included in Eq. 13 are attributed for hooked fibres. In the present method, numerical and experimental entities are simultaneously used, hence the experimental one was distinguished by an overline, i.e. $\overline{N}^i$ represents for the pullout force experimentally measured in the *i*-th scan read-out. Additionally, remark that for a smooth fibre $\overline{N} = N'(\tilde{L}_b)$, while for a hooked fibre $\overline{N} = N'(\tilde{L}_b) + N_{sp}$.

$$x = 0 \rightarrow \begin{cases} s(0) = s_f \\ N(0) = 0 \\ \varepsilon_f(0) = 0 \end{cases} \qquad x = \tilde{L}_b \rightarrow \begin{cases} s(\tilde{L}_b) = s_l \\ N(\tilde{L}_b) = \overline{N} \\ \varepsilon_f(\tilde{L}_b) = N'\left(\tilde{L}_b\right)/\left(E_f A_f\right) \end{cases} \tag{12}$$

$$x = 0 \rightarrow \begin{cases} s(0) = s_f \\ N(0) = N_{sp} \\ \varepsilon_f(0) = 0 \end{cases} \qquad x = \tilde{L}_b \rightarrow \begin{cases} s(\tilde{L}_b) = s_l \\ N(\tilde{L}_b) = \overline{N} \\ \varepsilon_f(\tilde{L}_b) = N'\left(\tilde{L}_b\right)/\left(E_f A_f\right) \end{cases} \tag{13}$$

The fibre pullout tests provide in terms of pullout force, $\overline{N}$, and loaded end slip, $\overline{s}_l$, several scan read-outs, being $\overline{s}_l^i$ and $\overline{N}^i$ the values of the *i*-th scan read-out. Regarding these experimental results, the set of unknown parameters of a given local bond relationship is desired to be found in order to fit the differential Eq. 4 as accurately as possible. A computational code was developed and implemented, supported on the algorithm described in Fig. 4. The second order differential Eq. 4 included in the algorithm is solved by the Runge-Kutta-Nyström (RKN) method. Further details of the latter method can be found elsewhere [19]. The algorithm is built up from the following main steps:

1. the $\tau - s$ relationship is defined attributing values to the unknown parameters. The error, $\overline{e}$, defined as the area between the experimental and analytical pullout force-slip curves, is initialized;
2. the numerical loaded end slip is calculated at the onset of the free end slip, $\tilde{s}_l$, (see Module A in Fig. 5);
3. for the experimental *i*-th scan reading, the loaded end slip, $\overline{s}_l^i$, and the pullout force, $\overline{N}$ are read;
4. taking the loaded end slip, $\overline{s}_l^i$, and using Eq. 4, the pullout force at the loaded end, $\overline{N}^i(s_l^i)$, is evaluated. In this case the following two loaded end slip conditions must be considered:
   - if $\overline{s}_l^i < \tilde{s}_l$, the determination of $\overline{N}^i(s_l^i)$ must take into account that the effective bond length is smaller than the fibre embedded length (see Module B on Fig. 5). For the case of hooked fibres, the mechanical anchorage contribution is not considered, since the fibre is not yet fully debonded;
   - if $\overline{s}_l^i \geq \tilde{s}_l$, the evaluation of $\overline{N}^i(s_l^i)$ is based on Module C (see Fig. 5). In this module, the contribution of the hooked end, $N_{sp}\left(s_l^i(\tilde{L}_b)\right)$, is assessed by an analytical expression, which was obtained by nonlinear fitting of experimental data, corresponding to the mechanical reinforcement mechanism of the hook.
5. the error associated with $\overline{N}^i(s_l^i)$ is calculated. This error is the area between the experimental ($A_{\text{exp},f}^i$) and numerical ($A_{num,f}^i$) curves. The points $\left(\overline{s}_l^{i-1}, N^{i-1}\left(s_l^{i-1}\right)\right)$ and $\left(\overline{s}_l^i, N^i\left(s_l^i\right)\right)$ are used to define the numerical curve, whereas the experimental curve is represented by the points

$\left(\bar{s}_l^{i-1}, \bar{N}^{i-1}\left(s_l^{i-1}\right)\right)$ and $\left(\bar{s}_l^{i}, \bar{N}^{i}\left(s_l^{i}\right)\right)$;

6. the error is updated.

In Modules B and C the Newton-Raphson method is used. Whenever the Newton-Raphson method fails, the bisection method is used as an alternative.

The determination of the unknown parameters defining the bond stress-slip relationship, $\tau - s$, was performed by a back-analysis, i.e. determining the $\tau - s$ relationship in such a way that the difference between the numerical and experimental pullout force-slip curves provides a minimum error, *e*. Additionally, two restriction conditions were added in order to assure similar values between the numerical and experimental peak pullout force and its corresponding slip (with a tolerance smaller than 2%). The back-analysis was performed by the exhaustive search method (brute force method), based on several parameters sets ascertained by a predefined range and step for each parameter of the corresponding set.

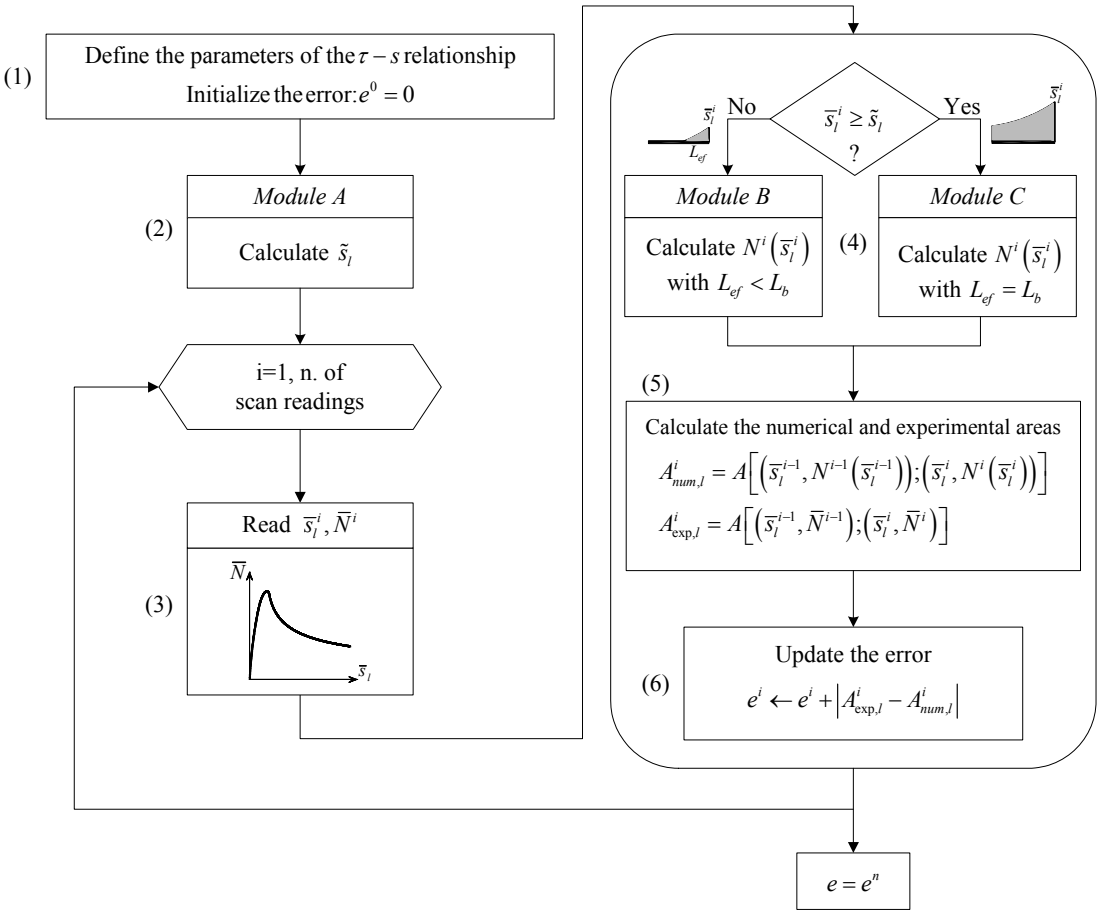


Figure 4: Algorithm implemented to obtain the local bond-stress slip relationship.

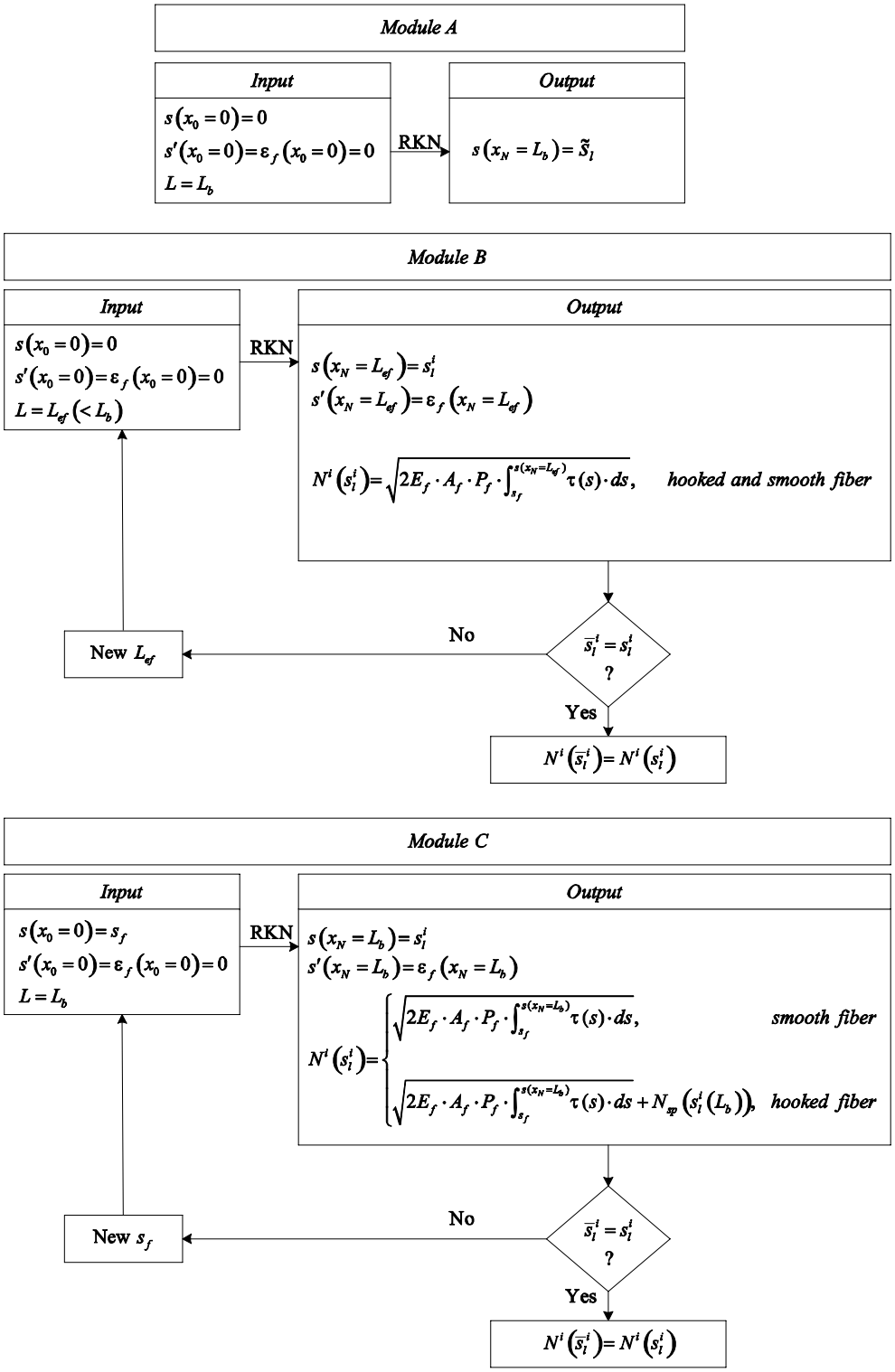


Figure 5: Modules A, B and C of the algorithm shown in Figure 4.

## 5 ASSESSMENT OF THE LOCAL BOND LAW FROM EXPERIMENTAL DATA

The present model was calibrated with both smooth and hooked-end steel fibres experimentally pulled-out from a steel fibre self-compacting concrete medium. The smooth fibres were tested with an embedment length of 20 and 30 mm, named, respectively, S_Lb20 and S_Lb30, whereas, the hooked fibres were tested with 10, 20 and 30 mm embedment length, and named H_Lb10, H_Lb20 and H_Lb30, respectively. Each series of smooth fibres comprised 3 specimens, whereas each series of hooked fibres included 6 specimens. A detailed description and discussion of the experimental test results, test setup, concrete composition, specimen preparation and other details is out of the scope of the present paper, and can be found elsewhere [20].

### 5.1 Analytical bond-slip relationship

The local bond stress-slip relationship used in the numerical simulations is given by Eq. 14, where $\tau_m$ and $s_m$ are, respectively, the bond strength and its corresponding slip. Parameter $\alpha$ defines the shape of the pre-peak branch, whereas $\alpha'$ and $s_1$ describe the configuration of the post-peak branch of the $\tau$-$s$ equation. These relationships were selected due to its easiness and aptitude to accurately model the local bond stress-slip behaviour, as previously ascertained by several researchers [18,21].

$$\tau(s) = \begin{cases} \tau_m \left(\dfrac{s}{s_m}\right)^{\alpha} \\ \tau_m \dfrac{1}{1+\left(\dfrac{s-s_m}{s_1}\right)^{\alpha'}} \end{cases} \tag{14}$$

### 5.2 Analytical relationship for the mechanical anchorage

The mechanical component of bond was obtained subtracting from the experimental average curve of the hooked series (curve 1, see Fig. 6), the correspondent experimental average curve of the smooth series (curve 2, see Fig. 6), i.e. the curves with the same embedment length. In a second step, an analytical relationship was obtained by nonlinearfitting of curve 3 (see Fig. 6) . A detailed description of this procedure is presented and discussed in [20].

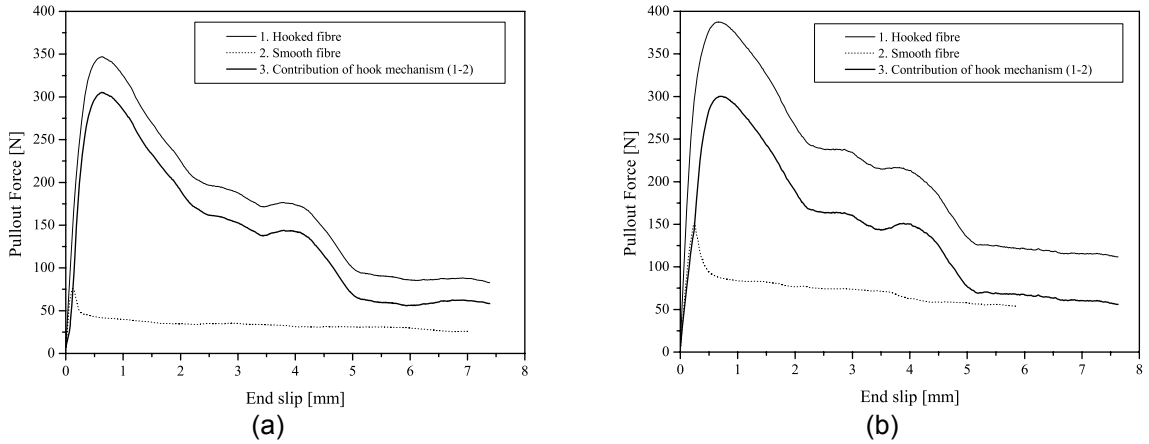


Figure 6: Contribution of the hooked-end to the overall pullout behaviour in fibre with an embedment length of: (a) 20 mm and (b) 30 mm.

### 5.3 Numerical simulation

The values of the parameters of the proposed local bond stress-slip relationship (see Eq. 14) were determined using the numerical strategy previously described. The local bond stress-slip relationship for each series was calibrated from the average experimental pullout force-slip curve. The values of the mechanical and geometric properties of the tested fibres used in the numerical simulation were the following: Young modulus, $E_f$, of 200 GPa; cross sectional area, $A_f$, of 0.562 mm$^2$; cross section perimeter, $P_f$, of 2.356 mm.

In Figs. 7 and 8 are depicted both the numerical pullout force-slip relationship and the experimental envelope for each tested series. On the other hand, the values of the parameters defining the local bond relationships, obtained by back analysis, are included in Table 1, as well as the corresponding normalised error, $\bar{e}$, which was defined as the ratio between $e$ and the area under the experimental curve. The numerical curves fitted the experimental data with high accuracy, even for high slip values, as the normalised error in each series is quite low. The average values and the corresponding coefficients of variation of the local bond law parameters are also indicated in Table 1. In spite of the accurateness of the numerical simulation, the coefficients of variation of the bond law parameters were quite high. This fact can be related to the method used in the back-analysis (exhaustive search), since the parameters search is based on a previously defined range and step, i.e. the parameter variables are discrete. Moreover, only one objective function was used, namely the difference between the area under the experimental and numerical curves, to determine the best fit for each series. A possible way to solve this problem could be the utilisation of a multi-objective function.

Table 1: Parameters for the local bond stress-slip relationship obtained by back analysis.

| Series | $s_m$ [mm] | $\tau_m$ [MPa] | $\alpha$ | $\alpha'$ | $s_1$ [mm] | $\bar{e}$ [%] |
|---|---|---|---|---|---|---|
| S_Lb20 | 0.14 | 1.77 | 0.60 | 0.22 | 0.44 | 3.2 |
| S_Lb30 | 0.24 | 2.27 | 0.69 | 0.42 | 1.30 | 5.0 |
| H_Lb10 | 0.25 | 1.61 | 0.22 | 0.88 | 0.53 | 4.3 |
| H_Lb20 | 0.23 | 1.80 | 0.84 | 0.45 | 1.10 | 2.2 |
| H_Lb30 | 0.14 | 2.10 | 0.89 | 0.42 | 2.21 | 1.9 |
| Average | 0.20 (24%) | 1.91 (11%) | 0.65 (37%) | 0.48 (45%) | 1.11 (57%) | - |

Values in round brackets are the coefficients of variation of the corresponding series.

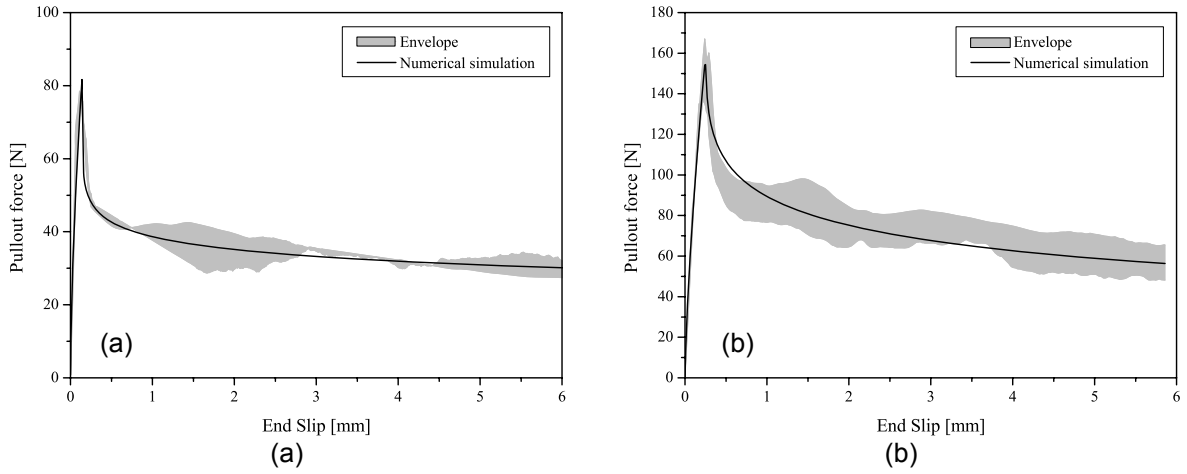


Figure 7: Pullout force-slip numerical simulation for a smooth fibre with an embedded length of: (a) 20 mm and (b) 30 mm.

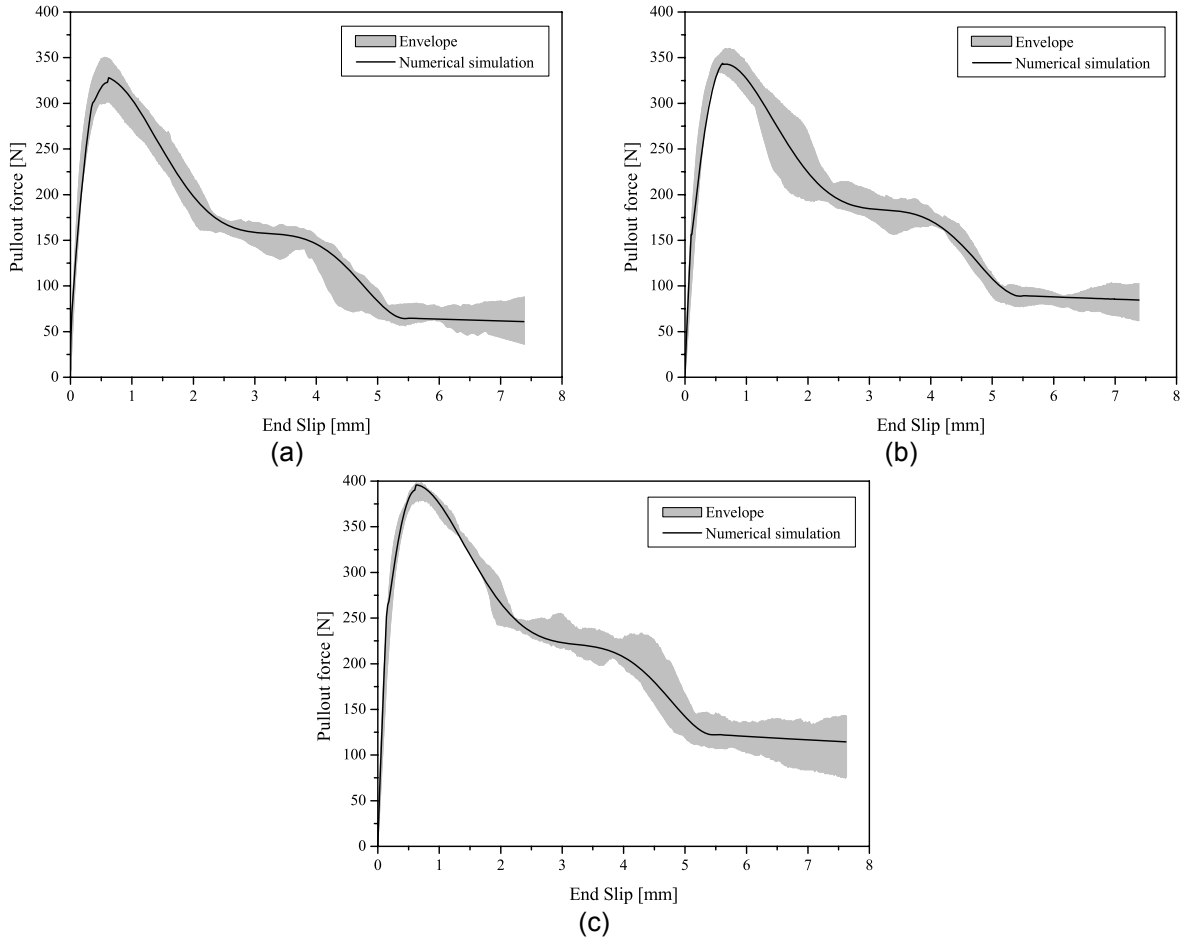


Figure 8: Pullout force-slip numerical simulation for a smooth fibre with an embedded length of: (a) 10 mm, (b) 20 mm and (c) 30 mm.

## 6 CONCLUSIONS

In the present work an analytical cohesive interface model was developed to obtain the bond stress-slip relationship for hooked ends steel fibres. To account for the progressive damage at the interfacial bond, a non-linear bond stress-slip law was used. On the other hand, the reinforcement mechanism provided by the fibre mechanical anchorage was accounted by a nonlinear spring component. The developed analytical model was able to simulate, with high accuracy, the experimental pullout force-slip curves, even for high slips for both hooked and smooth fibres. In spite of the accurateness of the numerical simulation, the coefficients of variation of the bond law parameters were quite high. This fact can be related to the method used in back-analysis (exhaustive search), since the parameters search strategy is based on a previously defined range and step, i.e the parameter variables are discrete. Moreover, it was used only one objective function, i.e. difference between the area under the experimental and numerical curves, to determine the best fit for each series. A possible way to solve this problem could be the utilisation of a multi-objective function. In spite of the high coefficients of variation for the local bond law parameters, some trends could be observed, such is the case of the increase of the bond strength parameter with the increase of the fibre embedment length.

## REFERENCES


[1] A. E. Naaman, H. Najm. Bond-slip mechanisms of steel fibres in concrete. ACI Materials Journal, 88(2): 135-145 (1991).

[2] N. Banthia, J. Tottier. Concrete reinforced with deformed steel fibres, Part I: Bond-slip mechanisms. *ACI Materials Journal*, 91(5): 435-446 (1994).

[3] H. Stang, Z. Li, S. P. Shah. Pullout problem: Stress versus Fracture Mechanical approach. *Journal of Engineering Mechanics*, 116(10): 2136-2150 (1990).

[4] A. E. Naaman, G. G. Namur, J. M. Alwan, H. S. Najm. Fiber pullout and bond slip I: Analytical study. *Journal of Structural Engineering ASCE*, 117(9): 2769-2790 (1990).

[5] J. M. Alwan, A. E. Naaman, P. Guerrero. Effect of mechanical clamping on the pull-out response of hooked steel fibres embedded in cementicious matrices. *Concrete Science and Engineering*, 1(1): 15-25 (1999).

[6] C. Sujivorakul, A. M. Waas, A. Naaman. Pullout response of a smooth fibre with an end anchorage. *Journal of Engineering Mechanics* ASCE, 126(9): 986-993 (2000).

[7] B. Banholzer, W. Brameshuber, W. Jung. Analytical simulation of pull-out tests – the direct problem. *Cement & Concrete Composites*, 27: 93-101 (2005).

[8] Lawrence, P. "Some theoretical considerations of fibre pull-out from an elastic matrix." *Journal of Materials Science*, 7(1): 1-7 (1972).

[9] Gopalaratnam, V. and Shah, S. P. "Failure mechanisms and fracture of fiber reinforced concrete." In *A. SP-105* (editor), "Fiber Reinforced Concrete Properties and Applications", 1-25. Oslo, Norway (1987).

[10] Wang, Y., Li, V. and Backer, S. "Modelling fiber pullout from a cement matrix." *International Journal of Cement Composites and Lightweight Concrete*, 10(3): 143-149 (1988).

[11] Leung, C. K. Y. and Li, V. "Effect of fiber inclination on crack bridging stress in brittle fiber reinforced brittle matrix composites." *Journal of Mechanics and Physics of Solids*, 40(6): 1333-1362 (1992).

[12] Li, V. C. and Stang, H. "Interface property characterisation and strengthening mechanisms in fibre reinforced cement based composites." *Advanced Cement Based Composites*, 6: 1-20 (1997).

[13] Robins, P., Austin, S. and Jones, P. "Pull-out behaviour of hooked steel fibres." *RILEM Journal of Engineering Mechanics*, 35(251): 434-442 (2002).

[14] Alwan, J. M., Naaman, A. E. and Guerrero, P. "Effect of mechanical clamping on the pull-out response of hooked steel fibers embedded in cementicious matrices." *Concrete Science and Engineering RILEM*, 1(1): 15-25 (1999).

[15] Sujivorakul, C., Waas, A. M. and Naaman, A. "Pullout response of a smooth fiber with an end anchorage." *Journal of Engineering Mechanics*, 126(9): 986-993 (2000).

[16] Russo, G., Zingone, G. and Romano, F. "Analytical solution for bond-slip of reinforcing bars in R.C. joints." *Journal of Structural Engineering ASCE*, 116(2): 336-355 (1990).

[17] Focacci, F., Nanni, A. and Bakis, C. "Local bond-slip relationship for FRP reinforcement in concrete." *Journal of Composites for Construction ASCE*, 4(1): 24-31 (2000).

[18] Sena-Cruz, J.M., Barros, J.A.O. "Modeling of bond between near-surface mounted CFRP laminate strips and concrete.",*Computers and Structures Journal*, 82(17-19), 1513-1521 (2004).

[19] Kreyszig, E. Advanced Engineering mathematics. John Wiley & Sons, Inc (1993).

[20] Cunha V. M. C. F., Barros J. A. O., Sena-Cruz J. Pullout behaviour of hooked-end steel fibres in self-compacing concrete. Technical report, 07-DEC/E-06, University of Minho, Portugal (2007).

[21] Stang, H. and Aarre, T. "Evaluation of crack width in FRC with conventional reinforcement." Cement & Concrete Composites, 14(1): 143-154 (1992).